DOI 10.1007/s11595-013-0759-5

The Effect of Elevated Temperature on Bond Performance of Alkali-activated GGBFS Paste

ZHENG Wenzhong, ZHU Jing*

(School of Civil Engineering, Harbin Institute of Technology, Harbin 150090, China)

Abstract: The main reaction products were investigated by analysis of microstructure of alkali-activated ground granulated blast furnace slag (GGBFS) paste. An experimental research was performed on bond performance of alkali-activated GGBFS paste as a construction adhesive after exposure to 20-500 ℃. Through XRD analysis, a few calcium silicate hydrate, hydrotalcite and tetracalcium aluminate hydrate were determined as end products, and they were filled and packed each other at room temperature. In addition, akermanite dramatically increased at 800 ℃ and above. The two key parameters, the ultimate load $P_{u.T}$ and effective bond length L_e, were determined using test data of carbon fiber-reinforced polymer (CFRP)-to-concrete bonded joints at elevated temperature. The experimental results indicate that the ultimate load $P_{u.T}$ remains relatively stable initially and then decreases with increasing temperature. The effective bond length L_e increases with increasing temperature except at 300 ℃. The proposed temperature-dependent effective bond length formula is shown to closely represent the test data.

Key words: alkali-activated GGBFS paste; microstructure; bond; effective bond length; elevated temperature

1 Introduction

Alkali-activated cementitious material[1] is a kind of cementitious material prepared by alkali-activator and pozzolanic or latent hydraulic material, which has been developed more than 70 years[2]. This material has attracted increasing attention because of their excellent mechanical properties[3,4], heavy metal ion solidification[5,6], thermostability[7], durability[8,9]. In addition, the preparation of the material conforms to the idea of sustainable development; a great upsurge on the research of this kind of material has been set off gradually in the world.

Alkali-activated ground granulated blast furnace slag (GGBFS) paste[10] and geopolymer[11] are the two main branches of alkali-activated cementitious material, they have common excellent characteristics, but the main disadvantages of geopolymer are he use of metakaolin (which is obtained by the calcination of kaolinite clay at a temperature ranging between 500 ℃ and 800 ℃) that is harmful to the environment, and the high curing temperature of geopolymers[12]. These problems could be solved if a GGBFS-based cementitious material is used instead of geopolymer, because the GGBFS is a valuable industrial by-product, and the alkali-activated GGBFS paste could be cured at room temperature.

In comparison to the epoxy resins, the alkali-activated GGBFS paste has shown superior thermal stability, and this material has a good potential for its future high-temperature applications in civil engineering[13]. Thus, it can become an eco-friendly fireproof substitute for epoxy resins, which soften quickly around their glass transition temperature T_g (generally in the range of 60 ℃ to 82 ℃)[14]. However, there have been few studies about the bond performance and thermal behavior of this material. In the present work, the ultimate load $P_{u.T}$ and failure modes of carbon fiber-reinforced polymer (CFRP)-to-concrete bonded joints as well as the effective bond length L_e were investigated. Results of this study provide a valuable reference for future design and

©Wuhan University of Technology and SpringerVerlag Berlin Heidelberg 2013

(Received: Dec. 19, 2012; Accepted: Feb. 21, 2013)

ZHENG Wenzhong(郑文忠): Prof.; E-mail: hitwzzheng@163.com

*Corresponding author: ZHU Jing(朱晶):Ph D Candidate;E-mail: zhujing02@126.com

Funded by the National Natural Science Foundation of China(50178026), and the Cheung Kong Scholars Program Foundation of Chinese Ministry of Education(2009-37)

construction applications.

2 Experimental

2.1 Materials

The raw materials of alkali-activated GGBFS paste were distilled water (H_2O), sodium hydroxide (NaOH), GGBFS and potassium silicate solution (K_2O•$nSiO_2$). The GGBFS was provided by Jingang Cement Exploiting Co., Ltd. The surface area and specific gravity of GGBFS were respectively 4 750 cm^2/g and 2.87 g/cm^3. The main compositions of GGBFS and potassium silicate solution are listed in Tables 1 and 2.

Table 1 Chemical compositions of GGBFS/%

SiO_2	Al_2O_3	CaO	MgO	TiO_2	FeO	MnO	K_2O
33.70	14.40	41.70	6.40	1.10	0.37	0.50	0.31

Table 2 Chemical compositions of $K_2O \cdot nSiO_2$

20 ℃		Modulus	wt/%	
Be	ρ/(g • cm^{-3})		K_2O	SiO_2
46.3	1.465	2.76	15.98	28.15

Note: Be=Baume degree, ρ=density, wt=weight ratio

Table 3 Mechanical properties of CFRP sheet

Aerial density /(g • m^{-2})	Nominal thickness /mm	Tensile strength /MPa	Young's modulus /MPa	Ultimate strain /%
300	0.167	4 125	244 000	1.71

CFRP sheet was provided by Japan Toray Co., Ltd. The mechanical properties of CFRP sheet are shown in Table 3. A concrete mix of Type I portland cement and aggregate with maximum size of 9.5 mm were used. The water-cement ratio by weight was 0.43. The compressive strength of concrete is 33.21 MPa. A total of 24 concrete prisms (800 mm×160 mm×160 mm) were fabricated in 6 series with each series having 4 specimens.

2.2 Specimens preparation

The specimens were prepared by mechanically mixing GGBFS, NaOH, H_2O and K_2O•$nSiO_2$ in a 5-L pan mixer. The optimum weight ratio was determinate as NaOH/GGBFS=0.05, H_2O/GGBFS =0.30 and K_2O•$nSiO_2$/GGBFS=0.19. The sequence of mixing was important to homogenize the fresh slurry. Thus, the GGBFS and alkaline-activator K_2O•$nSiO_2$ (the NaOH was dissolved in K_2O•$nSiO_2$ to adjust modulus) were firstly mixed for about 1 min at low speed, then H_2O was poured into the pan and stirred for approximately 6 min until the mixture was well combined.

The alkali-activated GGBFS specimens were cast as 40 mm × 40 mm × 160 mm prisms for measurement of microstructure. The ordinary portland cement (OPC) control specimens with a water/binder ratio of 0.25 were machined to the same size for comparison. They were cured in a humidistat at 20 ± 2 ℃ and 95% relative humidity. The inside surfaces of the moulds were coated with a water-based released agent to prevent the samples from sticking to the moulds surface during the steam curing process. The specimens were demolded after 24 h of humidity curing and then stored in a humidistat at 20 ± 2 ℃ and 50% relative humidity until testing commenced.

After 7 min of mechanical stirring, the homogeneous alkali-activated GGBFS slurry was transferred to a groove. For the CFRP-to-concrete bonded joints tests, the fibers were impregnated in the slurry and unidirectionally pestled using a smooth roller for 15 min. The reinforced fibers were then gently pressed into the uncured slurry on the concrete surface. The entrained air was removed using a plastic scraper. The specimens were covered with a film to prevent moisture loss and cured at room temperature for 28 days to develop mechanical properties.

2.3 Test methods

X-ray diffraction data were collected using a D/max-γB X-ray diffractometer (XRD, Rigaku, Japan). The specimens for XRD were prepared by first grinding them into an agate mortar and pestle until sufficiently small particle size was obtained. The specimen was then transferred to a glass slide and spread to a thin layer. The specimens were dried at room temperature for at least 1 h before running the XRD. In addition, the specimens after exposure to 20-1 200 ℃ were cooled down to room temperature naturally before running the XRD.

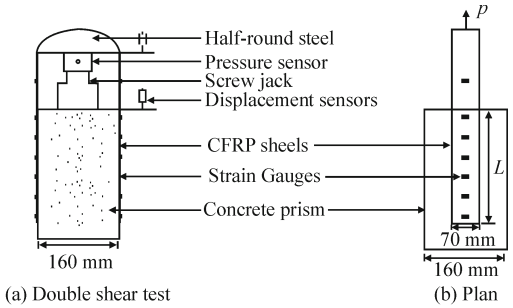

Fig.1 Layout of experiment

The CFRP-to-concrete bonded joints tests were performed using an electric furnace at six different target temperatures: 20 ℃, 100 ℃, 200 ℃, 300 ℃, 400 ℃, 500 ℃. The heating rate was set to 4 ℃/min. When the temperature inside furnace reached the target temperature, the temperature was kept for 2 h to make the specimens temperature homogenous. The

specimens were then cooled down to room temperature naturally in furnace. Finally, the specimens were taken out from the furnace and each of the symmetrical sides of the specimen was pasted with strain gauges. Stain gauges and displacement sensors were used to measure strains in the CFRP sheets and displacements at various positions, as shown in Fig.1.

3 Results and discussion

3.1 X-ray diffraction

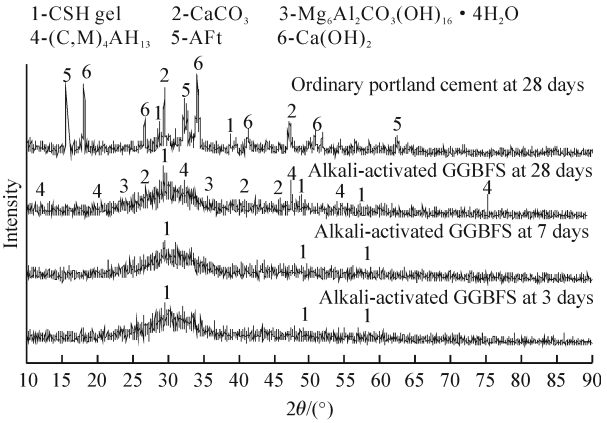

Fig.2 XRD patterns at room temperature

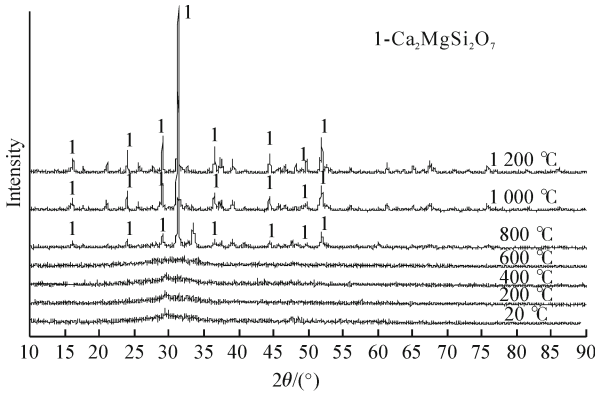

Fig.3 XRD patterns at elevated temperature

Fig.2 presents the XRD data at room temperature. There is some formation of calcium silicate hydrate (CSH) gel at 3 d; the characteristic diffraction peaks do not obviously change at 7 d . However, a few changes arouse until 28 d. This is because the large amount of amorphous materials appear in the slurry, the amount of initial generation CSH gel is small, and the GGBFS and $K_2O•nSiO_2$ in H_2O are consumed. A few hydrotalcite $[Mg_6Al_2CO_3(OH)_{16}•4H_2O]$ and tetracalcium aluminate hydrate $[(C,M)_4AH_{13}]$ can be produced, and they are filled and packed each other at room temperature. In addition, the main reaction products between alkali-activated GGBFS paste and OPC are very different, and the portlandite $[Ca(OH)_2]$ is easy to decompose. That is the reason why the OPC can not resist high temperature.

The characteristic diffraction peaks of CSH gel are obviously for the alkali-activated GGBFS specimen at 28 d (referring to Fig.2). While the peaks of CSH gel disappear after exposure to 800 ℃ (referring to Fig.3), simultaneously, the peaks of akermanite $[Ca_2MgSi_2O_7]$ increase significantly, which suggests that the thermostability and mechanical properties of alkali-activated GGBFS paste will deteriorate after exposure to 800 ℃ and above[13]. Fig.3 indicates that the akermanite peaks gradually increase, while CSH gel peaks gradually decrease with increasing temperature.

3.2 Failure modes and ultimate load

For double shear tests, there are five possible distinct failure modes in theory for CFRP sheets bonded to concrete after exposure to high temperature, although they may be mixed in an actual failure. These are listed below in the order of their likeliness, as is obvious from the results collected in Table 4.

1. Concrete failure
2. Concrete-to-adhesive interfacial failure
3. Adhesive failure
4. CFRP-to-adhesive interfacial failure
5. CFRP tensile rupture

Table 4 Double shear test data

No	Temperature T/℃	CFRP sheets		Failure mode
		Bond length L/mm	Ultimate load $P_{u,T}$/kN	
Ⅰ-1	20	180	22.20	CF
Ⅰ-2	20	200	23.65	CF
Ⅰ-3	20	220	24.35	CF
Ⅰ-4	20	240	24.38	CF
Ⅱ-1	100	200	21.64	CF
Ⅱ-2	100	220	22.39	CF
Ⅱ-3	100	240	23.17	CF
Ⅱ-4	100	260	23.21	CF
Ⅲ-1	200	220	20.37	CF
Ⅲ-2	200	240	21.19	CF
Ⅲ-3	200	260	22.15	CF
Ⅲ-4	200	280	22.19	CF
Ⅳ-1	300	240	23.54	CF
Ⅳ-2	300	260	23.57	CF
Ⅳ-3	300	280	23.58	CR
Ⅳ-4	300	300	23.60	CR
Ⅴ-1	400	260	17.05	CF
Ⅴ-2	400	280	18.21	CF
Ⅴ-3	400	300	18.86	CF
Ⅴ-4	400	320	18.89	CF
Ⅵ-1	500	320	15.11	CA
Ⅵ-2	500	340	16.02	CF
Ⅵ-3	500	360	16.72	CF
Ⅵ-4	500	380	16.75	CF

Note: CF=Concrete failure, CR=CFRP rupture, CA=CFRP-to-adhesive interfacial failure

Results show that most experimental joints fail in the concrete a few millimeters beneath the concrete-to-adhesive interface. A small number of specimens fail

by CFRP rupture, they are governed by the properties of the bonded CFRP sheets rather than the bond length. Concrete-to-adhesive interfacial failure and cohesive failure through adhesive are not found in Table 4. These are the consequence of the availability of alkali-activated GGBFS paste as strong adhesive that bonds well to CFRP sheets and concrete. For the same reason, CFRP-to-adhesive interfacial failure is rare, as only one such case is seen in Table 4, while it can be avoided by careful surface preparation to reinforced fibers.

A significant increase in ultimate load is noted with an increase in the bond length of CFRP sheets at three different temperatures (*i e*, 20, 100 and 200 ℃), however, there is a slight increase in ultimate load at three different temperatures (*i e*, 300, 400 and 500 ℃). The ultimate load of the CFRP-to-concrete bonded joints after exposure to high temperature is found to decrease by 4.85%, 9.03% and 3.32% when the temperature is increases from 20 ℃ to 100 ℃, 200 ℃ and 300 ℃, respectively. Besides, when the temperature further increases to 400 ℃ and 500 ℃, the ultimate loads decrease by 22.55% and 31.34%, respectively. This is because a continuous decrease in tensile strength of concrete prisms appears with increasing temperature.

3.3 Effective bond length

Fig.4 shows typical distributions of strains in the CFRP strip after high temperature. These strains are found from strain gauges mounted on the upper surface of the CFRP strip. When the applied load P is smaller than about 60% of the ultimate load $P_{u.T}$, the CFRP strain is minimal beyond a small distance of about $0.5L_e$ from the loaded end, indicating that almost all the applied load resist within this small area. At higher loads, the distribution of the applied load become more and more even in the initial bond zone. It may be noted that a large part of the CFRP strip near the far end still have minimal strain when the ultimate load reached, confirming the concept of effective bond length L_e implying that increasing the bond length L beyond a certain value L_e does not further increase the ultimate load $P_{u.T}$. In Fig.2, s is loaded end slip.

Based on fracture mechanics analysis[15,16], the fracture energy G_f at room temperature can be calculated by Eq.(1)

$$G_f = c_f f_{\text{ctm}} \tag{1}$$

where, f_{ctm} (MPa) is the concrete surface tensile strength, and c_f (mm) is an average value of 0.204 mm with a standard deviation of 0.053 for c_f for 51 specimens. Effective bond length L_e at room temperature can be calculated by Eq.(2)

$$L_e = \sqrt{\frac{E_p t_p}{2 f_{\text{ctm}}}} \tag{2}$$

where, E_p (MPa) and t_p (mm) are the Young's modulus and thickness of the CFRP sheets, respectively.

After exposure to high temperature, the fracture energy $G_{f,T}$[17] can be calculated by Eq.(3)

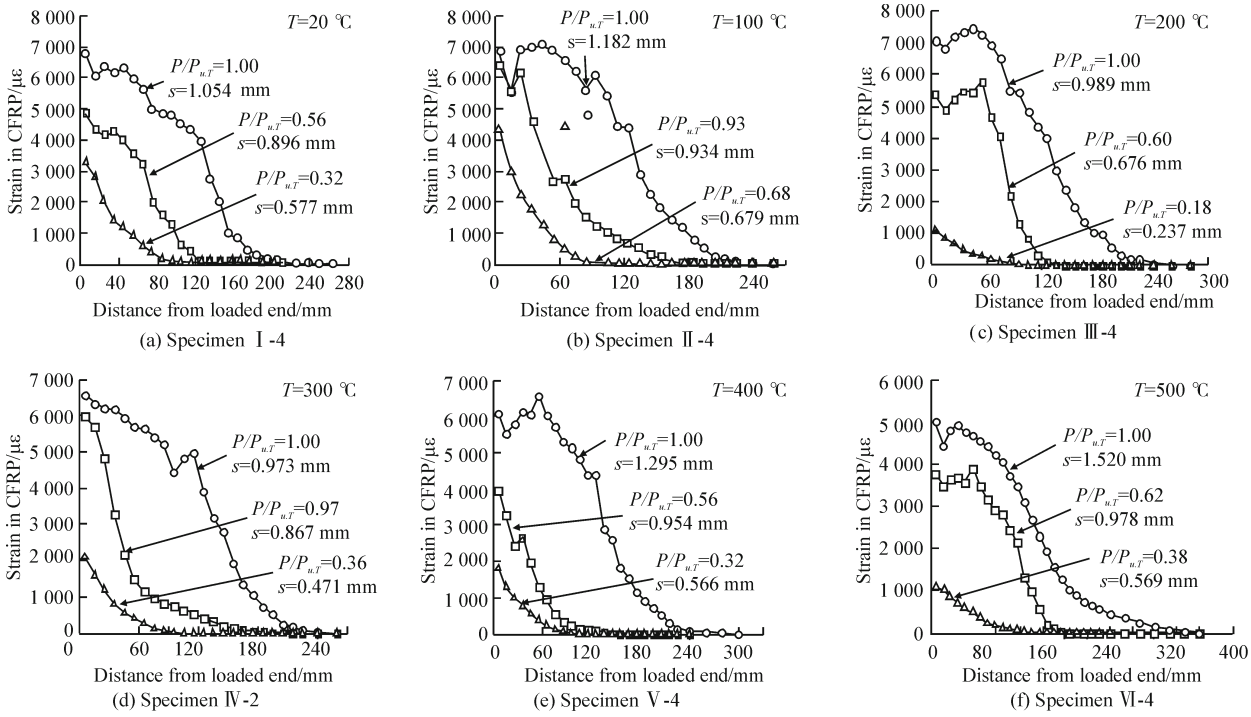

Fig.4 Effects of elevated temperature on strain distribution

$$G_{fT} = \frac{[P_{u.T} + \frac{\tau_f b_p}{\lambda_1^2 \delta_1}(\alpha_p - \alpha_c)\Delta T]^2}{2b_p^2 E_p t_p} \quad (3)$$

where, τ_f (MPa) is the maximum stress on the shear-slip curve of the bond; b_p is the width of the bonded CFRP strip; δ_1 (mm) is the τ_f corresponding slip; α_p and α_c (/℃) are the coefficients of heat expansion of CFRP sheets and concrete, respectively; λ_1 is defined by Eq.(4)

$$\lambda_1^2 = \frac{\tau_f}{\delta_1 E_p t_p}(1+\alpha_Y) \quad (4)$$

where, $\alpha_Y = \frac{b_p E_p t_p}{b_c E_c t_c}$, which is a stiffness ratio of the bonded joint; b_c (mm), E_c (MPa) and t_c (mm) are the width, Young's modulus and thickness of the concrete, respectively.

Fracture energy G_f was replaced by $G_{f,T}$, and the effective bond length L_e after exposure to high temperature is calculated by Eq. (5)

$$L_e = \frac{b_p E_p t_p \sqrt{c_f}}{\left| \frac{P_{u.T}}{4} + \frac{\tau_f b_p}{\lambda_1^2 \delta_1}(\alpha_p - \alpha_c)\sqrt{\Delta T} \right|} \quad (5)$$

In making the predictions, the following geometric and material properties are used: b_p= 70 mm, E_p=244000 MPa, t_p=0.167 mm, c_f=0.204 mm, τ_f=2.77 MPa, δ_1=0.02 mm, α_p=0.3×10-6/℃, α_c= 10.2×10^{-6}/℃, b_c=160 mm, E_c=30000 MPa, t_c= 160 mm. The effective bond length L_e increases with increasing temperature, except the temperature at 300 ℃ (referring to Fig.4), which could be deduced directly from Eq.(5).

4 Conclusions

a) XRD pattern analysis indicates that the thermostability and mechanical properties of alkali-activated GGBFS paste deteriorate after exposure to 800 ℃ and above. Thus, the alkali-activated GGBFS paste has potential applications in CFRP strengthened concrete structures at elevated temperature.

b) Experimental results suggest that the main failure mode is concrete failure beneath the concrete-to-adhesive interface. This is the consequence of the availability of alkali-activated GGBFS paste as strong adhesive that bonds well to CFRP sheets and concrete.

c) The elevated temperature has a significant effect. When the temperature is not higher than 300 ℃, the ultimate load of the CFRP-to-concrete bonded joint has little change compared with the original unheated. After exposure to 400-500 ℃, the ultimate load decreases with increasing temperature.

d) The effective bond length increases with increasing temperature except the temperature at 300 ℃, and a temperature-dependent effective bond length formula has been established and closely represent the test data.

References

[1] Shi CJ, Krivenko PV, Roy DM. Alkali-activated Cements and Concretes[M]. *London; Taylor & Francis*, 2006

[2] Luo X, Xu JY, Bai EL, *et al*. Systematic Study on the Basic Characteristics of Alkali-activated Slag-fly Ash Cementitious Material System[J]. *Construction and Building Materials*, 2012, 29: 482-486

[3] Roy DM, Jiang WM, Silsbee MR. Chloride Diffusion in Ordinary, Blended, and Alkali-activated Cement Pastes and Its Relation to Other Properties[J]. *Cement and Concrete Research*, 2000, 30(12): 1 879-1 884

[4] Guo WY, Wu GL, Wang JD, *et al*. Preparation and Performance of Geopolymers[J]. *Journal of Wuhan University of Technology-Mater. Sci. Ed*., 2008, 23(3): 326-330

[5] Bobrowski A, Gawlicki M, Malolepszy J. Analytical Evaluation of Immobilization of Heavy Metals in Cement Matrices[J]. *Environmental Science & Technology*, 1997, 31(3): 745-749

[6] Shi CJ, Fernandez-Jimenez A. Stabilization/ Solidification of Hazardous and Radioactive Wastes with Alkali Activated Cements[J]. *Journal of Hazardous Materials B*, 2006, 137(3): 1 656-1 663

[7] Barbosa VFF, MacKenzie KJD. Thermal Behaviour of Inorganic Geopolymers and Composites Derived from Sodium Polysialate[J]. *Materials Research Bulletin*, 2003, 38(2): 319-331

[8] Roy DM. Alkali-Activated Cements Opportunities and Challenges[J]. *Cement and Concrete Research*, 1999, 29(2): 249-254

[9] Bakharev T. Durability of Geopolymer Materials in Sodium and Magnesium Sulfate Solutions[J]. *Cement and Concrete Research*, 2005, 35(6): 1 233-1 246

[10] Richardson IG, Brough AR, Groves GW, *et al*. The Characterization of Hardened Alkali-activated Blast- furnace Slag Pastes and Nature of the Calcium Silicate Hydrate (C-S-H) Phase[J]. *Cement and Concrete Research*, 1994, 24(5): 813-829

[11] Davidovits J. Geopolymers Inorganic Polymeric New Materials[J]. *Journal of Thermal Analysis and Calorimetry*, 1991, 37(8): 1 633-1 656

[12] Muniz-Villarreal MS, Manzano-Ramirez A, Sampieri-Bulbarela S, *et al*. The Effect of Temperature on the Geopolymerization Process of a Metakaolin-based Geopolymer[J]. *Materials Letters*, 2011, 65(6): 995-998

[13] Zuda L, Rovnanik P, Bayer P, *et al*. Thermal Properties of Alkali-Activated Slag Subjected to High Temperatures[J]. *Journal of Building Physics*, 2007, 30(4): 337-350

[14] ACI 440.2R-08. *Guide for the Design and Construction of Externally Bonded FRP Systems for Strengthening Concrete Structures*[S]. Committee 440, USA, 2008

[15] Chen JF, Teng J. Anchorage Strength Models for FRP and Steel Plates Bonded to Concrete[J]. *Journal of Structural Engineering*, 2001, 127(7): 784-791

[16] Teng JG, Chen JF, Smith ST, *et al. FRP- Strengthened RC Structures* [M]. Chichester; John Wiley and Sons, 2002

[17] Dai JG, Gao WY, Teng JG. Bond-slip Model for FRP Laminates Externally Bonded to Concrete at Elevated Temperature [EB/OL]. http://dx.doi.org /10.1061/(ASCE)CC.1943-5614.0000337